ASYMPTOTIC GLOBAL CONFIDENCE REGIONS FOR 3-D PARAMETRIC SHAPE ESTIMATION IN INVERSE PROBLEMS

Jong Chul Ye[1]*, Pierre Moulin*[2]*, and Yoram Bresler*[2]

[1] Dept. of BioSystems, Korea Advanced Institute of Science and Technology, Daejeon, Korea
[2] Coordinated Science Lab, University of Illinois at Urbana-Champaign, USA

ABSTRACT

This paper derives fundamental performance bounds for estimating 3-D parametric surfaces in inverse problems. Unlike conventional pixel-based image reconstruction approaches, our problem is reconstruction of the shape of binary or homogeneous objects. The fundamental uncertainty of such estimation problems can be represented by global confidence regions, which facilitate geometric inference and optimization of the imaging system. Compared to two-dimensional global confidence region analysis in our previous work, computation of the probability that the entire 3-D surface estimate lies within the confidence region is, however, more challenging, because a surface estimate is an inhomogeneous random field continuously indexed by a two-dimensional index set. We derive an approximate lower bound to this probability using the so-called *tube formula* for the tail probability of a Gaussian random field. Simulation results demonstrate the tightness of the resulting bound and the usefulness of 3-D global confidence region approach.

1. INTRODUCTION

The problem of representing and reconstructing three dimensional surfaces has been a classical topic in computer vision, medical imaging, and graphics. A variety of representation techniques have been used for shape estimation; for example, nonuniform rational B-splines surfaces (NURBS) [1], extended Gaussian image (EGI) [2], or generalized cylinders [3]. Since a surface $\boldsymbol{S}$ is a two-dimensional manifold in $\mathbb{R}^3$, it is often represented as

$$\boldsymbol{S} = \mathbf{s}(\Psi) \stackrel{\triangle}{=} \{\mathbf{s}(\mathbf{t}) : \mathbf{t} \in \Psi\} \in \mathbb{R}^3 \tag{1.1}$$

where Ψ denotes a two-dimensional subset of $\mathbb{R}^2$, with boundary $\partial\Psi$ of zero Lebesgue measure.

We consider the following generic statistical model for estimation of a surface $\boldsymbol{S}$ from a collection of L noisy data vectors $\{\mathbf{y}_i\}$, which are independently distributed as:

$$\mathbf{Y}_i \sim p(\mathbf{y}_i|\boldsymbol{S}), \quad \mathbf{Y}_i \in \mathcal{Y}_1 \times \cdots \times \mathcal{Y}_M, \quad i = 1, \ldots, L \tag{1.2}$$

where $\boldsymbol{S}$ is given by (1.1), $\mathcal{Y}_m$ denotes the observation space for the m-th component $\mathbf{Y}_i(m)$ of $\mathbf{Y}_i$, $p(\mathbf{y}_i|\boldsymbol{S})$ is the probability density function describing the observation model, and M is the number of components in each observation. Such problems are encountered in applications such as computer vision, computed tomography (CT), deconvolution, synthetic aperture radar (SAR), and nonlinear inverse scattering. The measurement model (1.2) encompasses situations of multisensor fusion or multimodality measurements, where different components of the vector $\mathbf{Y}_i$ are produced by different sensors, each with its own measurement space $\mathcal{Y}_m$.

We often represent the surface $\boldsymbol{S}$ parameterically,

$$\mathbf{s}(\mathbf{t}) = \mathbf{s}(\mathbf{t}; \boldsymbol{\theta}) \tag{1.3}$$

where the K-dimensional parameter vector

$$\boldsymbol{\theta} = \begin{bmatrix}\theta_1 & \cdots & \theta_K\end{bmatrix}^T \in \boldsymbol{\Theta} \subset \Psi \tag{1.4}$$

The mapping $\mathbf{s} : \Psi \times \mathbb{R}^K \rightarrow \mathbb{R}^3$ of (1.3) can be nonlinear. An advantage of such finite parametric representations is that they alleviate the ill-posedness of inverse problems. Furthermore, they reduce the surface estimation problem to the estimation of the finite dimensional parameter $\boldsymbol{\theta}$ from the combined data set $\mathbf{Y}$, where the two are related by the probability law $\mathbf{Y} \sim p(\mathbf{y}|\boldsymbol{\theta})$ obtained from (1.2) and (1.3).

Our goal in this paper is to develop tools for the prediction and assessment of the quality of the estimates $\mathbf{s}(\mathbf{t}; \hat{\boldsymbol{\theta}})$ from the measurement model (1.2). Although the well-known Cramèr-Rao inequality [4] can be used to predict and assess the quality of the parameter estimator $\hat{\boldsymbol{\theta}}$, one is more interested in assessing the quality of estimates in easily interpreted geometric terms. Rather than the quality of estimates of $\boldsymbol{\theta}$ itself, what is needed is a *global* quality measure for the entire surface. Such quantification of the uncertainty in shape and surface estimation problems may answer questions such as: what accuracy can be expected at any given point, which features of a shape are difficult to estimate, what is the effect of different parameterizations and data collecting geometries, etc.

Working on a two-dimensional parametric shape estimation problem, Ye, Bresler and Moulin [5] proposed a

technique for constructing small-size *global confidence regions* in the asymptotic regime where the estimate is unbiased, efficient, and Gaussian, and provided bounds on the probability that the entire boundary estimate lies in the global confidence region. These confidence regions can be conveniently visualized, see Fig. 1 for a 2-D example. They incorporate limits on the estimation performance for interesting geometric parameters such as shape, size, orientation, and the position of the object into an uncertainty band $\mathcal{U}_\beta$. The parameter β trades off the size of the uncertainty band against the probability that the true shape belongs to that band. Then, one can investigate the fundamental performance of shape estimation from the geometric properties of the confidence regions. The usefulness of the global confidence region analysis was demonstrated in imaging applications such as nonlinear inverse scattering problems, computed tomography, Fourier imaging, deconvolution, computer vision, and discrete tomography [6, 7, 8, 9].

There are significant difficulties, however, in obtaining a geometrically meaningful global performance measure for 3D surface estimation. The main one is that the surface estimate $\hat{\mathbf{s}}(\mathbf{t}) = \mathbf{s}(\mathbf{t}; \hat{\boldsymbol{\theta}})$ is a *random field* continuously indexed by a two dimensional variable $\mathbf{t}$. Therefore, statistical analysis of surface estimates is harder than the 2-D global confidence region analysis [5], in which the estimate is a 1-D random process.

The main contribution of this paper is to derive the global confidence level using the so-called *tube formula* [10] for the tail probability of nonhomogeneous Gaussian random fields. This guarantees that the entire actual surface asymptotically lies in the global confidence region formed around the maximum-likelihood estimate of the surface, with the calculated probability.

2. MAIN RESULT

To set up the problem and its solution, we summarize some background material from our previous work on global confidence regions [5]. At each location $\mathbf{t} \in \Psi$, we can derive a confidence region for the maximum-likelihood estimator $\mathbf{s}(\mathbf{t}; \hat{\boldsymbol{\theta}})$. A confidence region is the likely range of the true value, and gives an indication of how much uncertainty there is in our estimate. The smaller the region, the more precise the estimate. Confidence regions are expressed in terms of a confidence level – the probability that the true value lies within the confidence region.

According to classical estimation theory [11], for *a fixed* $\mathbf{t}$, a confidence region $\hat{\mathcal{U}_\beta}(\mathbf{t})$ for $\mathbf{s}(\mathbf{t}; \boldsymbol{\theta})$ at confidence level $\alpha \in [0,\ 1]$ is any subset of $\mathbb{R}^3$ such that

$$\Pr\Big\{\mathbf{s}(\mathbf{t}) \in \hat{\mathcal{U}_\beta}(\mathbf{t})\Big\} \quad = \quad \alpha\,. \tag{2.5}$$

Of all possible choices of $\hat{\mathcal{U}_\beta}(\mathbf{t})$ for each specified α, the smallest size confidence region is [12]

$$\hat{\mathcal{U}_\beta}(\mathbf{t}) \quad = \quad \Big\{\mathbf{x} \in \mathbb{R} \,:\, ||\mathbf{x} - \hat{\mathbf{s}}(\mathbf{t})||^2_{\mathbf{C_s}(\mathbf{t})^{-1}} \le \beta^2\Big\} \tag{2.6}$$

for an appropriate $\beta > 0$, where $\mathbf{C_s}(\mathbf{t})$ is the error covariance matrix for $\mathbf{s}(\mathbf{t}; \hat{\boldsymbol{\theta}})$. Note that for each $\mathbf{t}$, the local confidence region in (2.6) is an ellipsoid in $\mathbb{R}^3$. The parameter β measures the lengths of the principal axes of this ellipsoid in units of standard deviation of the estimation error along these axes. This is a *local* confidence region, because (for each t) it only applies to one point of the surface.

We now construct a global confidence region $\hat{\mathcal{U}_\beta}$ for the entire surface $\boldsymbol{S} = \{\mathbf{s}(\mathbf{t}), \forall\, \mathbf{t} \in \Psi\}$:

$$\hat{\mathcal{U}_\beta} \quad \triangleq \quad \bigcup_{\mathbf{t}\in\Psi} \hat{\mathcal{U}_\beta}(\mathbf{t})\,. \tag{2.7}$$

Note that the construction of $\hat{\mathcal{U}_\beta}$ is similar to morphological dilation of the boundary by the spatially varying structuring element $\hat{\mathcal{U}_\beta}(\mathbf{t})$. Therefore, the region $\hat{\mathcal{U}_\beta}$ forms a "thick shell" around the estimated boundary $\hat{\mathbf{s}}(\mathbf{t})$.

Modifying the local confidence level (2.5) to acommodate the probabilistic interpretation of $\hat{\mathcal{U}_\beta}$, the global confidence level for $\hat{\mathcal{U}_\beta}$ is given by:

$$\gamma \triangleq \Pr\Big\{\ \boldsymbol{S} \in \hat{\mathcal{U}_\beta}\ \Big\} = \Pr\Big\{\mathbf{s}(\mathbf{t}) \in \hat{\mathcal{U}_\beta},\ \forall\, \mathbf{t} \in \Psi\Big\}\ . \tag{2.8}$$

This is the probability that the entire surface lies within the region $\hat{\mathcal{U}_\beta}$ formed around the surface estimate.

A dual probability is

$$\gamma' \triangleq \Pr\Big\{\ \hat{\boldsymbol{S}} \in \mathcal{U}_\beta\ \Big\} = \Pr\{\ \hat{\mathbf{s}}(\mathbf{t}) \in \mathcal{U}_\beta,\ \forall\, \mathbf{t} \in \Psi\ \} \tag{2.9}$$

where $\hat{\mathbf{s}}(\mathbf{t})$ is the estimate of $\mathbf{s}(\mathbf{t})$, and the deterministic confidence region $\mathcal{U}_\beta$ is defined as

$$\mathcal{U}_\beta \quad \triangleq \quad \bigcup_{\mathbf{t}\in\Psi} \mathcal{U}_\beta(\mathbf{t})\,, \tag{2.10}$$

where $\mathcal{U}_\beta(\mathbf{t})$ is given by

$$\Big\{\mathbf{x} \in \mathbb{R} : (\mathbf{x} - \mathbf{s}(\mathbf{t}))^T\, \mathbf{C_s}(\mathbf{t})^{-1}\, (\mathbf{x} - \mathbf{s}(\mathbf{t})) \le \beta^2\ \Big\}\,. \tag{2.11}$$

Again, the region $\mathcal{U}_\beta$ is a shell, but this time centered on the true boundary. While γ of (2.8) is the *a posteriori* probability that the true shape lies in a confidence region generated around the MLE $\hat{\boldsymbol{S}}$, the *a priori* probability γ' of (2.9) predicts the fundamental uncertainty region for *any* asymptotically normal and efficient estimator. The posterior confidence region $\hat{\mathcal{U}_\beta}(\mathbf{t})$ and its associated probability are computed after the measurements are collected and the MLE $\hat{\mathbf{s}}(\mathbf{t})$ determined. The *a priori* confidence region $\hat{\mathcal{U}_\beta}$ and its associated probability are computed without any measurements, and are only based on the *a priori* model $\mathbf{s}(\mathbf{t}; \boldsymbol{\theta})$ and

(1.2). Therefore, in general they are different, and each has its distinct applications.

By deriving an explicit formula for γ, (or for γ') we can compute the corresponding value of β in (2.6) (respectively, in (2.11)) for the prescribed global confidence level γ (γ') and guarantee the probability that the true surface (resp. the MLE) lies within the confidence region. The goal of this paper is to determine approximate bounds on γ and γ' that are reasonably tight.

2.1. Canonical Coordinates

Now, we return to our main interest: bounds on the probabilities (2.8). These probabilities satisfy the following inequalities:

$$\gamma \stackrel{\triangle}{=} \Pr\left\{ \mathbf{s}(\mathbf{t}) \in \hat{\mathcal{U}_\beta} \right\} \geq \Pr\left\{ \mathbf{s}(\mathbf{t}) \in \hat{\mathcal{U}_\beta}(\mathbf{t}) \right\} \stackrel{\triangle}{=} \gamma_{\rm LB} \quad (2.12)$$

$$\gamma' \stackrel{\triangle}{=} \Pr\{ \hat{\mathbf{s}}(\mathbf{t}) \in \mathcal{U}_\beta \} \geq \Pr\{ \hat{\mathbf{s}}(\mathbf{t}) \in \mathcal{U}_\beta(\mathbf{t}) \} \stackrel{\triangle}{=} \gamma'_{\rm LB} \quad (2.13)$$

Note the difference between the left-hand sides and the corresponding lower bounds on right-hand sides in (2.12) and (2.13). For example, while γ in (2.12) is the probability that the surface lies within the global confidence region $\hat{\mathcal{U}_\beta}$ – which is not a function of $\mathbf{t}$, $\gamma_{\rm LB}$ on the right is the probability that all points of the surface lie within their respective local confidence regions $\hat{\mathcal{U}_\beta}(\mathbf{t})$. The inequalities are true, because in the case of (2.12) there may exist some $\mathbf{t} \neq \mathbf{t}'$ such that $\mathbf{s}(\mathbf{t}) \in \hat{\mathcal{U}_\beta}(\mathbf{t}')$ (and therefore, by the definition of $\mathcal{U}_\beta$, $\hat{\mathbf{s}}(\mathbf{t}) \in \mathcal{U}_\beta$) while $\mathbf{s}(\mathbf{t}) \notin \hat{\mathcal{U}_\beta}(\mathbf{t})$, with the analogous situation for (2.13). Now, owing to the definitions (2.6) and (2.11), $\gamma_{\rm LB}$ and $\gamma'_{\rm LB}$ are asymptotically identical because $\hat{\mathbf{C}}_{\mathbf{s}}$ approaches $\mathbf{C}_{\mathbf{s}}$. Therefore, in the sequel we derive approximations for $\gamma'_{\rm LB}$ as a means to obtain, at the same time, asymptotic lower bounds on both γ and γ'.

Define the transformed parameter-vector

$$\mathbf{Z} \stackrel{\triangle}{=} \mathbf{C}_{\boldsymbol{\theta}}^{-1/2} \left(\hat{\boldsymbol{\theta}} - \boldsymbol{\theta} \right) \in \mathbb{R}^K \quad (2.14)$$

which is asymptotically normally distributed: $\mathbf{Z} \sim \mathcal{N}(\mathbf{0}, \mathbf{I})$. Then, $\gamma'_{\rm LB}$ can be expressed in terms of the random vector $\mathbf{Z}$ by

$$\gamma'_{\rm LB} = \Pr\{ \mathbf{Z}^T \mathbf{P}(\mathbf{t}) \mathbf{Z} \leq \beta^2, \forall\, \mathbf{t} \in \Psi \}, \quad (2.15)$$

where $\mathbf{P}(\mathbf{t})$ is the projection matrix onto the range space of $\mathbf{C}_{\boldsymbol{\theta}}^{1/2} \mathbf{B}(\mathbf{t})$ given by

$$\mathbf{P}(\mathbf{t}) \stackrel{\triangle}{=} \mathbf{C}_{\boldsymbol{\theta}}^{1/2} \mathbf{B}(\mathbf{t}) \left(\mathbf{B}(\mathbf{t})^T \mathbf{C}_{\boldsymbol{\theta}} \mathbf{B}(\mathbf{t}) \right)^{-1} \mathbf{B}(\mathbf{t})^T \mathbf{C}_{\boldsymbol{\theta}}^{1/2}. \quad (2.16)$$

Note that the rank of $\mathbf{P}(\mathbf{t})$ is equal to $\eta \leq 3$. The problem is thus reduced to finding an approximation for the right-hand side of (2.15).

2.2. The Exceedence Probability Bound

A more accurate approximation for $\gamma'_{\rm LB}$ is derived by taking into account the characteristics of $\mathbf{C}_{\boldsymbol{\theta}}^{1/2} \mathbf{B}(\mathbf{t}) \in \mathbb{R}^{K \times 3}$. Let $\mathbf{Q}(\mathbf{t}) = [\mathbf{q}_1, \cdots, \mathbf{q}_\eta]$ be the $K \times \eta$ matrix with orthonormal columns spanning the range space of $\mathbf{C}_{\boldsymbol{\theta}}^{1/2} \mathbf{B}(\mathbf{t})$ (obtained, e.g., by a QR decomposition of $\mathbf{C}_{\boldsymbol{\theta}}^{1/2} \mathbf{B}(\mathbf{t})$). It follows that

$$\mathbf{Z}^T \mathbf{P}(\mathbf{t}) \mathbf{Z} = \mathbf{Z}^T \mathbf{Q}(\mathbf{t}) \mathbf{Q}^T(\mathbf{t}) \mathbf{Z} = \|\mathbf{G}(\mathbf{t})\|^2, \quad (2.17)$$

where $\mathbf{G}(\mathbf{t}) \stackrel{\triangle}{=} \mathbf{Q}^T(\mathbf{t}) \mathbf{Z} \in \mathbb{R}^\eta$. Consider the following Gaussian random field :

$$X(\mathbf{t}, \boldsymbol{\omega}) \stackrel{\triangle}{=} \mathbf{d}^T(\boldsymbol{\omega}) \mathbf{G}(\mathbf{t}) = \mathbf{d}^T(\boldsymbol{\omega}) \mathbf{Q}^T(\mathbf{t}) \mathbf{Z}, \quad (2.18)$$

where the set $\{\mathbf{d}(\boldsymbol{\omega}) \in \mathbb{R}^\eta, \boldsymbol{\omega} \in \Omega \subset \mathbb{R}^{\eta-1}\}$ is the η-dimensional unit sphere; here $\boldsymbol{\omega}$ denotes spherical coordinates. By defining a new argument

$$\boldsymbol{\tau} = (\mathbf{t}, \boldsymbol{\omega}) \in T = \Psi \times \Omega \subset \mathbb{R}^N \quad (2.19)$$

where

$$N = \eta - 1 + dim(\Psi) = \eta + 1 \quad (2.20)$$

(for $\Psi \subset \mathbb{R}^2$, in the case of surfaces in 3-D) and using the condition for equality in the Cauchy-Schwarz inequality for $\mathbf{G} \in \mathbb{R}^\eta$, we have,

$$\|\mathbf{G}(\mathbf{t})\| = \sup_{\substack{\mathbf{d} \in \mathbb{R}^\eta \\ \|\mathbf{d}\|=1}} [\mathbf{d}^T \mathbf{G}(\mathbf{t})] = \sup_{\boldsymbol{\omega} \in \Omega} X(\mathbf{t}, \boldsymbol{\omega}), \quad (2.21)$$

hence

$$\begin{aligned} \gamma'_{\rm LB} &= \Pr\{ \mathbf{Z}^T \mathbf{P}(\mathbf{t}) \mathbf{Z} \leq \beta^2, \forall\, \mathbf{t} \in \Psi \} \\ &= \Pr\left\{ \sup_{\mathbf{t} \in \Psi} ||\mathbf{G}(\mathbf{t})|| \leq \beta \right\} \\ &= \Pr\left\{ \sup_{\mathbf{t}, \boldsymbol{\omega}} X(\mathbf{t}, \boldsymbol{\omega}) \leq \beta \right\} \\ &= 1 - \Pr\left\{ \sup_{\mathbf{t}, \boldsymbol{\omega}} X(\mathbf{t}, \boldsymbol{\omega}) \geq \beta \right\} \\ &= 1 - \Pr\left\{ \sup_{\boldsymbol{\tau} \in T} X(\boldsymbol{\tau}) \geq \beta \right\}. \end{aligned} \quad (2.22)$$

Therefore, our problem has been reduced to evaluation of the following exceedence probability (or tail probability) for a random field:

$$\Pr\left\{ \sup_{\boldsymbol{\tau} \in T} X(\boldsymbol{\tau}) \geq \beta \right\}. \quad (2.23)$$

In spite of its apparent simplicity, the determination of the exceedence probability of (2.23) is a notoriously difficult problem. According to Adler [13], there are only six cases in which the exact formula for the exceedence probability (2.23) are known. Other than these, only approximate solutions are available, and there are a multitude of different techniques, in particular for large β [13, 14, 15, 16, 17, 18].

2.2.1. The Tube Formula

Owing to the special geometric structure of $X(\boldsymbol{\tau})$, we can use the following, powerful *tube formula* [10], which provides a precise asymptotic expansion of (2.23) as $\beta \to \infty$. Examples of manifolds without boundary include hyperspheres and tori.

Theorem 2.1 (Sun [10]) *Let $X(\boldsymbol{\tau})$ be a nonsingular Gaussian random field on a N-dimensional Borel measurable set $T \subset \mathbb{R}^N$ with mean 0, variance 1 and covariance function $r(\mathbf{s}, \boldsymbol{\tau})$. If $r(\mathbf{s}, \boldsymbol{\tau}) \in C^3$ has finite Karhunen-Loève expansion*

$$r(\mathbf{s}, \boldsymbol{\tau}) = \sum_{i=1}^{K} u_i(\mathbf{s}) u_i(\boldsymbol{\tau}) \ , \ K < \infty \ , \tag{2.24}$$

and the manifold $\mathcal{U} = \{(u_1(\boldsymbol{\tau}), \cdots, u_K(\boldsymbol{\tau})), \boldsymbol{\tau} \in T\}$ has no boundary, then as $\beta \to \infty$,

$$\begin{aligned} Pr\left\{ \sup_{\boldsymbol{\tau} \in T} X(\boldsymbol{\tau}) \geq \beta \right\} &= \kappa_0 \psi_0(\beta) + \kappa_2 \psi_2(\beta) + \cdots \\ &\quad + \kappa_{\tilde{N}} \psi_{\tilde{N}}(\beta) + o(\psi_{\tilde{N}}(\beta)) \end{aligned} \tag{2.25}$$

where $\tilde{N} = N$ for even N and $\tilde{N} = N - 1$ for odd N, respectively. Here

$$\begin{aligned} \psi_n(\beta) &= \frac{1}{2^{1+n/2} \pi^{(N+1)/2}} \int_{\beta^2/2}^{\infty} u^{(N+1-n)/2-1} e^{-u} \, du \ , \\ &\quad n = 0, 2, \cdots, \tilde{N} \ . \end{aligned} \tag{2.26}$$

and $\kappa_0, \cdots, \kappa_{\tilde{N}}$ are the constants in Weyl's formula [19] for the manifold $\mathcal{U}$.

Discussion: The constants κ_0 and κ_2 are geometric descriptors of the K-dimensional differentiable manifold $\mathcal{U}$. More specifically, κ_0 denotes the volume (or area) of the manifold $\mathcal{U}$ and κ_2 is a total scalar curvature:

$$\kappa_0 = |\mathcal{U}| = \int_T ||\mathbf{R}(\boldsymbol{\tau})||^{1/2} d\boldsymbol{\tau} \tag{2.27}$$

$$\kappa_2 = \int_T \left(-\frac{C}{2} - \frac{N(N-1)}{2} \right) ||\mathbf{R}(\boldsymbol{\tau})||^{1/2} d\boldsymbol{\tau} \tag{2.28}$$

where $||\mathbf{R}(\boldsymbol{\tau})||$ denotes the determinant of the *metric tensor matrix* $\mathbf{R}(\boldsymbol{\tau})$ given by

$$\mathbf{R}(\boldsymbol{\tau}) = (g_{ij}(\boldsymbol{\tau}))_{N \times N} \tag{2.29}$$

$$g_{ij}(\boldsymbol{\tau}) = \sum_{l=1}^{K} \frac{\partial u_l(\boldsymbol{\tau})}{\partial t_i} \frac{\partial u_l(\boldsymbol{\tau})}{\partial t_j} = \left. \frac{\partial^2 r(\mathbf{s}, \boldsymbol{\tau})}{\partial s_i \partial \tau_j} \right|_{\mathbf{s}=\boldsymbol{\tau}} \tag{2.30}$$

In (2.28), C is the intrinsic scalar curvature of the manifold, which is zero for homogeneous random fields. Usually, the computation of C for inhomogeneous random fields (such as $X(\boldsymbol{\tau})$) is quite complicated as it requires the computation of Christoffel symbols and Ricci curvature tensor. Therefore, we use the following one-term asymptotic approximation.

Due to the special structure of $X(\boldsymbol{\tau})$, we can easily prove that the Gaussian random field $X(\boldsymbol{\tau}) = X(\mathbf{t}, \boldsymbol{\omega})$ in (2.18) satisfies the assumptions of Theorem 2.1. Therefore, we have the following result.

Proposition 2.2 (Ye et al[20]) *Suppose $\mathbf{s}(t; \boldsymbol{\theta})$ is three times differentiable. Then,*

$$\begin{aligned} \gamma'_{\mathrm{LB}} &= Pr\left\{ \mathbf{s}(\mathbf{t}, \hat{\boldsymbol{\theta}}) \in \mathcal{U}_\beta(\mathbf{t}), \ \forall \, \mathbf{t} \in \Psi \right\} \\ &= 1 - \frac{\kappa_0}{\omega_N} \left(1 - \Gamma\left(\frac{N+1}{2}, \frac{\beta^2}{2} \right) \right) \left[1 + O(\beta^{-2}) \right] \\ \omega_N &= \frac{2 \, \pi^{(N+1)/2}}{\Gamma(\frac{N+1}{2})} \end{aligned}$$

where κ_0, and $\mathbf{R}(\boldsymbol{\tau})$ are given by (2.27)*, and* (2.29)*.*

3. NUMERICAL RESULTS

We now examine the problem of 3-D Fourier imaging from sparse samples. We will assume a binary object. Consider a boundary $\partial\Omega = \{\mathbf{s}_0(\mathbf{t}; \boldsymbol{\theta}) : \mathbf{t} \in \Psi\}$ in the form of a nominal torus

$$\mathbf{s}_0(\mathbf{t}) = \mathbf{s}_0(u, v) = \begin{bmatrix} (R + r\cos(v))\cos(u) \\ (R + r\cos(v))\sin(u) \\ -r\sin(v) \end{bmatrix} \ , \tag{3.1}$$

where R denotes the radius from the center of the hole to the center of the torus tube, and r is the radius of the tube. A more general torus can be obtained by rotation and translation:

$$\mathbf{s}(\mathbf{t}) = \boldsymbol{\mathcal{R}}_x(\phi) \boldsymbol{\mathcal{R}}_y(\psi) \mathbf{s}_0(\mathbf{t}) + \boldsymbol{\mathcal{T}} \tag{3.2}$$

where $\boldsymbol{\mathcal{R}}_x(\phi)$ and $\boldsymbol{\mathcal{R}}_y(\psi)$ are the rotation matrices with respect to the x and y axes with angles ϕ and ψ, respectively[1] ; and $\boldsymbol{\mathcal{T}}$ is the translation offset given by

$$\boldsymbol{\mathcal{T}} = \begin{bmatrix} p_x & p_y & p_z \end{bmatrix}^T \ . \tag{3.3}$$

Knowing that the object to be imaged is a torus, and assuming that the geometrical parameters of the rotated and translated torus are unknown, the shape estimation problem reduces to estimating the vector parameter $\boldsymbol{\theta} \in \mathbb{R}^7$:

$$\boldsymbol{\theta} = \begin{bmatrix} \phi & \psi & r & R & p_x & p_y & p_z \end{bmatrix}^T \ . \tag{3.4}$$

[1] Note that the nominal torus in (3.1) has the z-axis as its symmetry axis. Any affine transform of the torus is completely described by the rotation and translation of this symmetry axis.

For example, Fig. 2(a) shows the torus with parameters given by

$$\boldsymbol{\theta} = \begin{bmatrix} \frac{\pi}{6} & 0 & 2 & 15 & 5 & 3 & 5 \end{bmatrix}^T . \quad (3.5)$$

The shape depends nonlinearly on $\boldsymbol{\theta}$, and the measurement depends nonlinearly on all the geometric parameters. Therefore, the MLE is only asymptotically unbiased, Gaussian, and efficient, and $\gamma'_{\mathrm{LB}} \rightarrow \gamma_{\mathrm{LB}}$ only asymptotically. Furthermore, for the parametrization in (3.1) and (3.2) the uncertainty is in all directions, and therefore none of the inequalities in (2.12) and (2.13) reduce to equalities. Since the global confidence region bound of Proposition 2.2 has been derived based on asymptotic arguments, the bound may not be accurate for smaller number of measurement samples. It does however become more accurate as the sample size increases. In order to illustrate this property, we take N^3 measurements by uniformly sampling the (k_x, k_y, k_z) cube, $[-0.5, 0.5]^3$. The i-th sample along any coordinate axis, say k_x direction is given by

$$k_x(i) = \frac{i+1}{N+1} - \frac{1}{2}, \quad i = 0, \cdots, N-1.$$

We choose N to be odd so as to include the DC component of the Fourier transform.

To proceed, we use a simple extension of the domain derivative techniques for computation of the CRB in 2-D shape estimation problems [7], to produce an explicit formula for the Fisher information matrix:

$$\left(\mathbb{I}_{\boldsymbol{\theta}}\right)_{i,j} = \frac{1}{\sigma^2} \sum_{m=1}^{N^3} \left[\left(\frac{\partial g_m(\boldsymbol{\theta})}{\partial \theta_i} \right)^* \frac{\partial g_m(\boldsymbol{\theta})}{\partial \theta_j} \right] \quad (3.6)$$

where

$$\frac{\partial g_m(\boldsymbol{\theta})}{\partial \theta_j} = \int_{\partial\Omega} e^{-i2\pi(k_x(m)x + k_y(m)y + k_z(m)z)} \langle \mathbf{b}_j, \boldsymbol{\nu} \rangle \, \boldsymbol{\nu} dS \ , \quad (3.7)$$

dS denotes a differential surface element, $\boldsymbol{\nu}$ is the outer-normal vector on the surface $\partial\Omega$, and

$$\mathbf{b}_j(u,v) = \frac{\partial \mathbf{s}(u,v)}{\partial \theta_j} . \quad (3.8)$$

The confidence region $\mathcal{U}_\beta$ is then computed by application of the expressions in (2.11), and (2.10), where the noise variance is set to $\sigma^2 = 10$ in order to demonstrate considerable thickness of the uncertainty region. For this choice of parameters, the global confidence region $\mathcal{U}_\beta$ with parameter $\beta = 5$ is shown in Fig. 2(b). Compared to the original torus, we see that the thickness of the uncertainty region is uneven, and that some areas are more difficult to estimate.

Next we compute the approximate bound on the global confidence level γ' and compare it with Monte-Carlo simulation results.

Fig. 3 depicts the exceedence probability approximation, incomplete gamma bound, and the Monte-Carlo simulation for $N = 9$ (accordingly, the number of samples is 9^3). Here, we do not display the lower bound becausee it is a lower bound on an upper bound on γ'_{LB} in the asymptotic region and is not guaranteed to be a lower bound on γ' in the nonasymptotic region. The exceedence probability approximation is quite accurate. Hence, we can conclude that even for a nonlinear parametrization our asymptotic global confidence region analysis gives a correct estimate of performance as long as we have a sufficient number of samples.

4. CONCLUSIONS

We have constructed a global confidence region within which the entire 3D shape estimate resides with a prescribed probability. The geometric properties of the global confidence region convey information about which parts of the shape are difficult to estimate and can be used to optimize imaging system parameters. The 3-D problem is quite challenging due to the fact that the shape estimate is a nonstationary random field over a multidimensional index set. Owing to the special structure of this random field, Sun's tube formula can be applied; we found this formula very useful for deriving the exceedence probability approximation. We also found that the new approximation is a generalization of the simple incomplete bounds for large number of unknown parameter cases. Based on the theoretical results and several test applications, this technique may prove useful in applications of parametric surface estimation to CT, MRI, and computer vision.

5. REFERENCES

[1] G. Farin, *Curves and Surfaces for Computer Aided Geometric Design*. San Diego, California: Academic Press, 4th ed. ed.

[2] B. Horn, "Extended Gaussian images," *Proc. of the IEEE*, vol. 72, pp. 1656–1678, December 1984.

[3] K. Kanatani, "Statistical bias of conic fitting and renormalization," *IEEE Trans. on Pattern Analysis and Machine Intelligence*, vol. 16, pp. 320–326, March 1994.

[4] H. L. VanTrees, *Detection, Estimation and Modulation Theory, Part I: Detection, Estimation, and Linear Modulation Theory*. New York: John Wiley & Sons, Inc., 1968.

[5] J. C. Ye, Y. Bresler, and P. Moulin, "Asymptotic global confidence regions in parametric shape estimation problems," *IEEE Trans. on Information Theory, Special Issue on Information Theoretic Imaging*, pp. 1881–1895, August 2000.

[6] J. C. Ye, Y. Bresler, and P. Moulin, "Cramér-Rao bounds for 2-D target shape estimation in nonlinear inverse scattering problems with application to passive radar," *IEEE Trans. on Antennas and Propagat.*, pp. 771–783, May 2001.

[7] J. C. Ye, Y. Bresler, and P. Moulin, "Cramér-Rao bound of parametric shape estimation in inverse problems," *IEEE Trans. on Image Processing*, pp. 71–84, January 2003.

[8] T. Tasdizen and R. Whitaker, "Cramer-Rao bounds for nonparametric surface reconstruction from range data," Tech. Rep. UUCS-03-006, University of Utah, School of Computing, April 2003.

[9] A.Poonawala, P. Milanfar, and R. Gardner, "A statistical analysis of shape reconstruction from areas of shadows," in *Proceedings of the 36th Asilomar Conference on Signals, Systems and Computers*, (Pacific Grove, CA), November 2002.

[10] J. Sun, "Tail probabilities of the maxima of Gaussian random fields," *Ann. Probab.*, vol. 21, pp. 34–71, January 1993.

[11] E. Lehmann and G. Casella, *Theory of Point Estimation*. New York: Springer-Verlag, 2nd ed., 2003.

[12] S. S. Wilks and J. F. Daly, "An optimum property of confidence regions associated with the likelihood function," *Ann. Math. Statist.*, no. 10, pp. 225–235, 1939.

[13] R. J. Adler, "On excursion sets, tube formulae, and maxima of random fields," *Annals of Applied Probability*, no. 1, pp. 1–74, 2000.

[14] V. I. Piterbarg, "High excursions for nonstationary generalized chi-square processes," *Stochastic Processes and their Applications*, no. 53, pp. 307–337, 1994.

[15] K. J. Worsley, "Local maxima and the expected Euler characteristic of excursion sets of χ^2, F and t fields," *Advances in Applied Probability*, no. 26, pp. 13–42, 1994.

[16] K. J. Worsley, "Boundary corrections for the expected Euler characteristic of excursion sets of random fields, with an application to astrophysics," *Advances in Applied Probability*, no. 27, pp. 943–959, 1995.

[17] K. J. Worsley, "Estimating the number of peaks in a random field using the Hadwiger characteristic of excursion sets, with applications to medical images," *Annals of Statistics*, no. 23, pp. 640–669, 1995.

[18] J. Cao and K. J. Worsley, "The detection of local shape changes via the geometry of Hotelling's t^2 fields," *Annals of Statistics*, in press.

[19] H. Weyl, "On the volume of tubes," *Amer. J. Math*, no. 61, pp. 461–472, 1939.

[20] J. C. Ye, P. Moulin, and Y. Bresler, "Asymptotic global confidence regions for 3-d parametric shape estimation in inverse problems," *IEEE Trans. on Image Processing*, submitted.

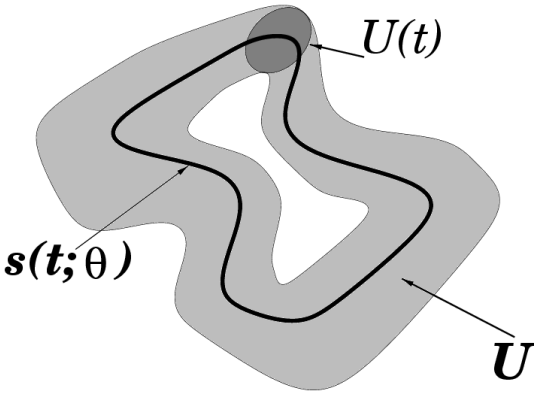

Fig. 1. Illustration of the global confidence region for a 2-D shape estimation problem [5] .

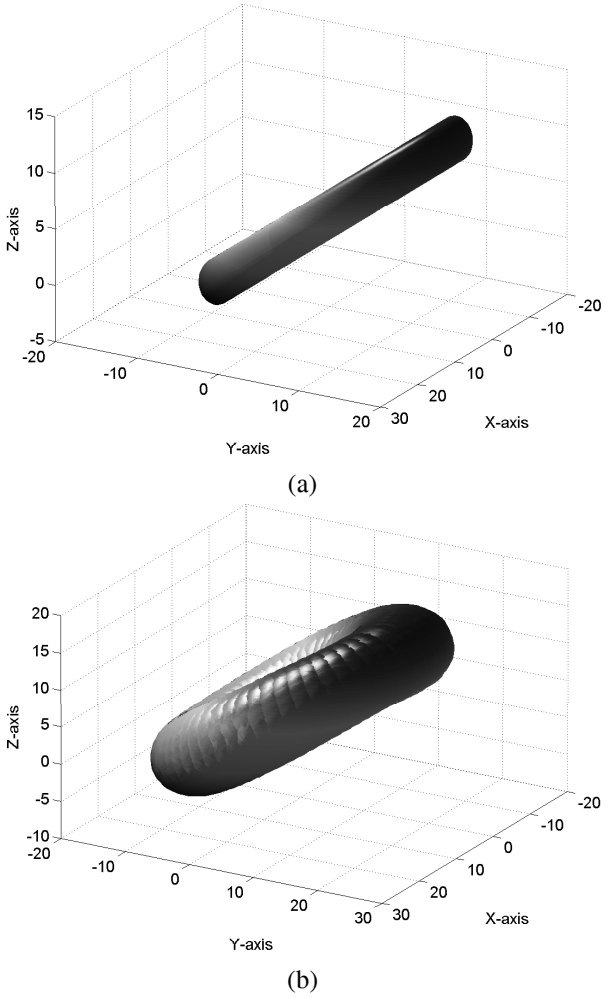

Fig. 2. (a) Torus with parameters of (3.5), and (b) global confidence region of the torus in Fig. 2 in a Fourier imaging problem.

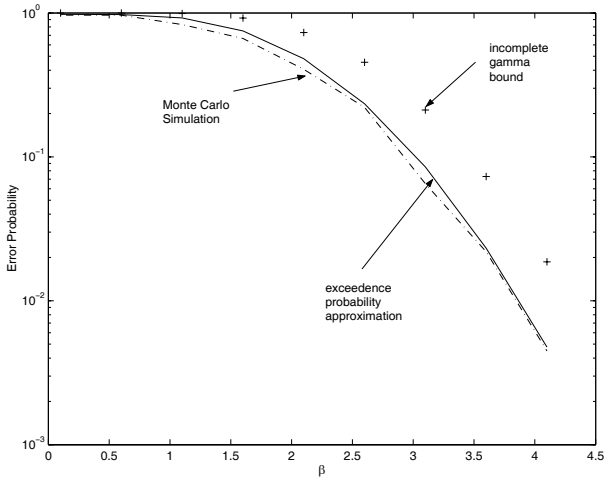

Fig. 3. Comparison of Monte-Carlo simulations, the exceedence probability approximation, and the incomplete Gamma-bound in the Fourier imaging problem for the sample size of 9^3.